ACS APPLIED ENERGY MATERIALS

www.acsaem.org Article

3D Printed SnS_2/SnS-Based Nanocomposite Hydrogel as a Photoenhanced Triboelectric Nanogenerator

Nishat Kumar Das, Sushmitha Veeralingam, and Sushmee Badhulika*

Cite This: ACS Appl. Energy Mater. 2023, 6, 6732−6741 Read Online

ACCESS | Metrics & More | Article Recommendations | Supporting Information

ABSTRACT: Recent advancements in printing technologies have led to new fabrication techniques for the development of various flexible, compact, wearable, and portable energy harvesters and self-powered devices. In particular, the three-dimensional printing (3DP) technology for a nanogenerator has become advantageous due to its low cost, simplicity, and high precision in fabricating complicated structures. Therefore, we report a 3DP-based photoinduced triboelectric nanogenerator (PTNG) fabrication, a hybrid version of a conventional triboelectric nanogenerator. Here, a 3D printed poly(vinyl alcohol) (PVA) nanocomposite hydrogel (3DPH) with photoactive SnS_2/SnS nanoflakes is used as a tribo-positive material and copper foil as a tribo-negative material for PTNG application. Under light illumination, the as-fabricated PTNG with an optimized weight percentage of SnS_2/SnS displays the open-circuit voltage (V_{oc}) enhancement from 29 to 37.5 V and short-circuit current (I_{sc}) enhancement from 1.23 to 1.58 μA. In addition, the power density of the device is observed at 5.4 $\mu W/cm^2$ under illumination conditions at the external load of 60 MΩ. This enhanced performance of the as-fabricated PTNG is attributed to the mutual coupling effect and improved interfacial interactions between the SnS_2/SnS nanoflakes and PVA under the influence of light illumination, leading to a charge-trapping mechanism. The outstanding performance and stability of the as-fabricated PTNG surpassing all similar recent reports, establish it as an effective hybrid platform for constructing multifunctional self-powered devices.

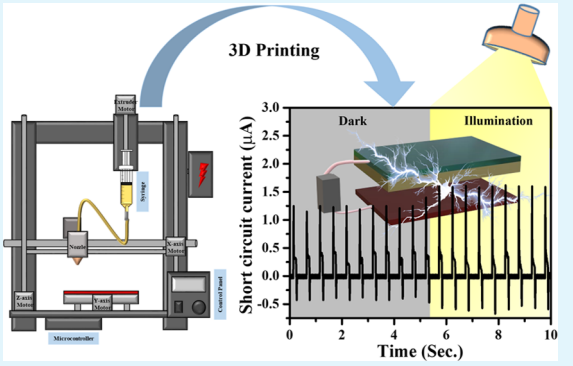

KEYWORDS: *triboelectric nanogenerator, 3D printing, SnS_2/SnS nanoflakes, nanocomposite hydrogel, photoinduced triboelectric nanogenerator*

1. INTRODUCTION

The rapid advancements in printing technology have received significant attention over the past few decades in different fields of applications, namely, printed electronics,[1] sensors,[2] biomedical,[3] and energy devices.[4] Generally, printed electronics are reported with enhanced properties like functionalities and efficacy of the devices. Such advancement in printing technology has been achieved through various printing methods such as screen, inkjet, and laser printing. However, these techniques are limited to two dimensions (2D) (i.e., *X*- and *Y*-axis), and a passive substrate is essential for device fabrication. To overcome this limitation of 2D printing and to enable easy fabrication of devices, the three-dimensional (3D) (i.e., *X*-, *Y*-, and *Z*-axis) printing technology has evolved. In this, the printing of the devices takes place in all three dimensions through a layer-by-layer deposition process, which does not require any passive substrate for device fabrication. In addition to this, it is also a cost-effective rapid device fabrication technique with high stability, sustainability, and efficiency than other printing devices.

Nanomaterial-based self-powered, portable electronic devices are widely reported for various applications like sensors, implants, etc. Generally, these devices are self-powered using nonconventional energy generation sources like mechanical,[4,5] thermal,[6] magnetic,[7] and photon[8] sources in their respective environments. Triboelectric nanogenerator uses mechanical energy as a source of energy generation. It converts mechanical energy to electrical by using two working principles: (i) contact electrification and (ii) electrostatic induction.[9] Contact electrification is otherwise known as triboelectrification, which is achieved via a friction mechanism between two dissimilar surfaces of identical or nonidentical materials using the concept of surface charge and the electron affinity of the surface.[10] Triboelectric nanogenerators are the eco-friendly,[11] cost-effective[12] energy harvesting platform reported with high efficacy[13] for small-scale energy harvesting applications. Though these devices have been explored for a wide variety

Received: April 6, 2023
Accepted: May 29, 2023
Published: June 14, 2023

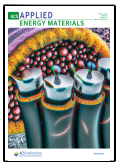

https://doi.org/10.1021/acsaem.3c00887
ACS Appl. Energy Mater. 2023, 6, 6732−6741

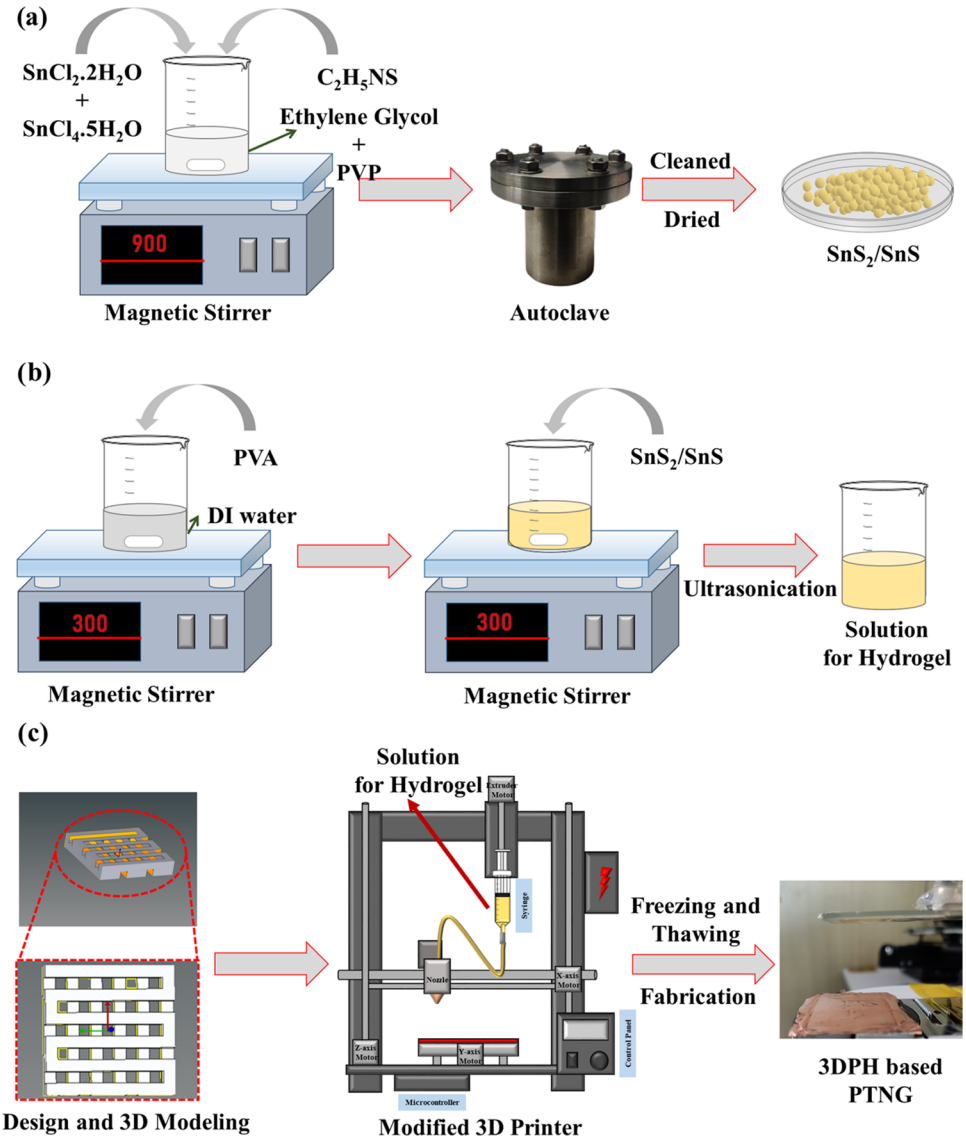

Figure 1. (a) Schematic of synthesis of SnS_2/SnS via a one-step solvothermal process. (b) Preparation of the SnS_2/SnS/PVA nanocomposite solution. (c) 3D printing of the SnS_2/SnS/PVA nanocomposite hydrogel.

of self-powered applications, efforts are made to enhance their overall efficiency and reliability.[14] The significant parameters to improve the device compatibility and efficiency are (i) material selection with significant differences of tribal-polarity,[13] (ii) charge injection,[15] (iii) hybridization with piezoelectric nanogenerator,[16] (iv) micro/nanopatterning to increase the contact area,[17] and (v) uses of photomodulated semiconductor material.[18,19] Among these strategies, using a photoactive semiconductor material is a new field of study in energy harvesting via triboelectric nanogenerators in the presence of photon illumination, known as photon-induced triboelectric nanogenerators (PTNGs). Han et al. have reported Au (metal) and TiO_2 (semiconductor) as tribo-negative and tribo-positive layers of a triboelectric nanogenerator, respectively, where the conductivity of the surface increased via photon illumination.[19] However, the device exhibited a low V_{oc} and I_{sc}. The energy conversion efficiency in photomodulated triboelectric nanogenerators depends on the optimum optical band gaps of the semiconductor material used.[20] The two major requirements of a material to be used in PTNGs are (i) a low energy band gap and (ii) high physical and chemical stability.

Transition-metal dichalcogenides (TMDCs) have been widely reported for different optoelectronics applications due to their high absorption coefficient and tunable energy band gaps. In particular, tin-based TMDCs are commonly used in optoelectronic devices as they exhibit n-type semiconductance in SnS_2 and p-type semiconductance in SnS with an energy band gap between 1.3 and 2.2 eV.[21,22] Therefore, the SnS_2/SnS exhibits a comparatively better electron-transport property and absorption coefficient than the common TiO_2 nanomaterials for optoelectronic applications.[23] On the other hand, polymer-based nanocomposites are also being used in PTNG applications due to their synergetic effect leading to a mutual coupling effect between the nanomaterials and the polymer matrix under light illumination. In addition, the morphology of the nanomaterial and interfacial characteristics of the polymer nanocomposite (i.e., interfacial interactions between the nanomaterial and the polymer matrix) leads to nanocomposites' improved dielectric, optical, and electrical properties.[24] Among various polymer nanocomposites, poly(vinyl alcohol) (PVA)-based composites exhibit high transparency and conductivity.[25]

https://doi.org/10.1021/acsaem.3c00887
ACS Appl. Energy Mater. 2023, 6, 6732−6741

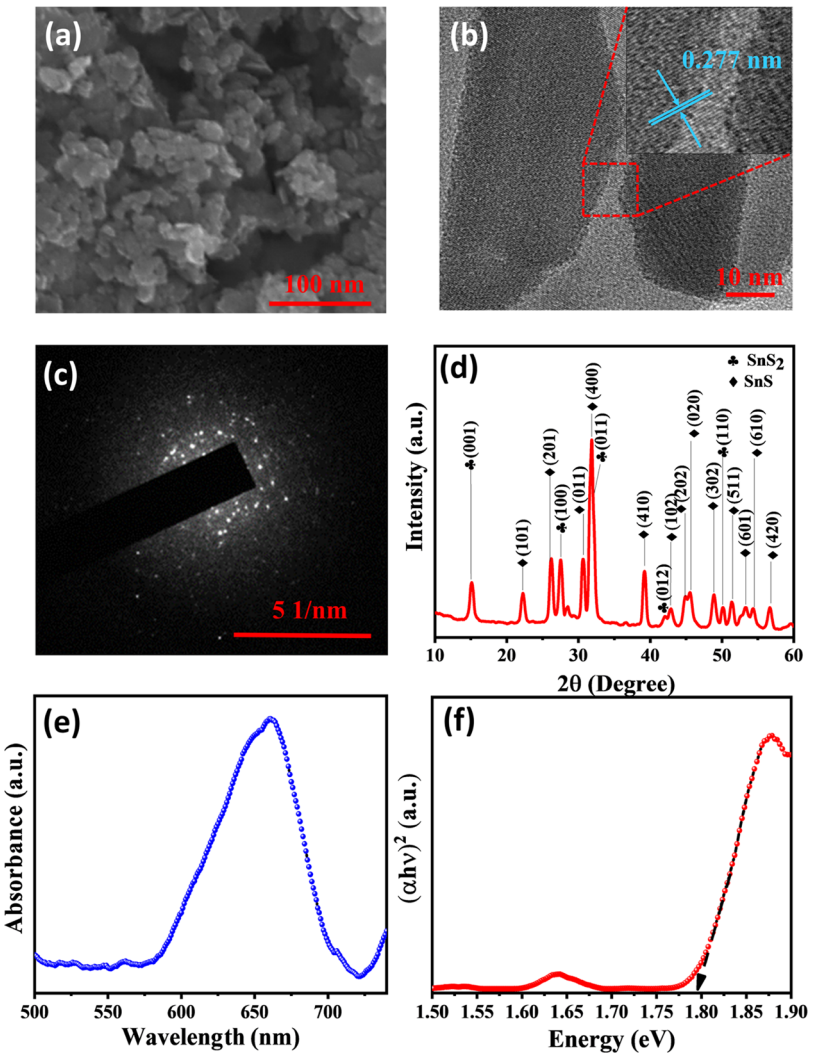

Figure 2. (a) SEM, (b) HR-TEM, (c) SAED pattern, (d) XRD, (e) UV−vis absorption spectrum, and (f) Tauc's plot of SnS_2/SnS.

In this work, we report a photoinduced triboelectric nanogenerator (PTNG) using 3D printed SnS_2/SnS-based PVA hydrogel (3DPH) as a photoactive tribo-positive material and copper foil as a tribo-negative material. The wt % of SnS_2/SnS in 3DPH has been optimized to 10 wt % based on triboelectric nanogenerator's energy conversion efficiency. In the dark, the 10 wt % SnS_2/SnS-loaded 3DPH-based triboelectric nanogenerator with a 2 cm × 2 cm active area generates a high V_{oc} and I_{sc}, i.e., 29.0 V and 1.23 μA, respectively. Upon illumination, V_{oc} and I_{sc} increase by 29 and 28%, which is 37.5 V and 1.58 μA, respectively. This increased output can be ascribed to the photoelectron or hole generation via photon illumination. Here, the photogenerated carriers help to trap charge by mutual coupling effect under illumination, which generates more surface charges. This work provides a new approach to fabricating a PTNG via a 3D printed light absorption layer with enhanced energy conversation efficiency.

2. MATERIALS AND INSTRUMENTATION

2.1. Materials. Tin chloride ($SnCl_2{\cdot}2H_2O$ (99.99%)), tin(IV) chloride ($SnCl_4{\cdot}5H_2O$ (98%)), thioacetamide (C_2H_5NS (99.99%)), ethylene glycol (anhydrous, 99.8%), poly(vinylpyrrolidone) (PVP, $(C_6H_9NO)_n$) poly(vinyl alcohol) (PVA, M_w 89,000-98,000, 99+% hydrolyzed), indium tin oxide coated poly(ethylene terephthalate) (ITO-PET) sheet (≤10 Ω sq^{-1}), and copper (foil, thickness 0.25 mm) were bought from Sigma Aldrich, India. Millipore setup (Merck, Direct Q 3-UV) was used for DI water.

2.2. Instrumentation. Structural analysis of the material was carried out using an X-ray diffractometer (XRD, Bruker Discover D8 with Cu Kα radiation). A scanning electron microscope (SEM, ApreoLoVac with additional EDS detector) and transmission electron microscope (TEM, JEM F200, JEOL Ltd.) were used to get the information about morphology. A Raman spectrometer (Witec, α-300) was also used to characterize the synthesized sample and understand the chemical structure. The composite films were 3D printed by a customized Creality Ender 3 V2 3D printer. All of the electrical characterization (output voltage and output current) measurements were measured by a digital storage oscilloscope (Agilent Technologies, DSO 3062A) and Source meter (Keithley, Tektronix, 2450). A Holmark ozone-free arc lamp (HO-SC-SS300C) was used as a light source.

3. EXPERIMENTAL SECTION

3.1. Synthesis of SnS_2/SnS Nanoflakes. SnS_2/SnS nanoflakes were synthesized via a facile one-step solvothermal method, as shown in Figure 1a. $SnCl_2{\cdot}2H_2O$, $SnCl_4{\cdot}5H_2O$, and C_2H_5NS were mixed in a 1:1:2 molar ratio with 30 mL of ethylene glycol. Then, the solution was stirred for 3 h after adding a small amount of PVP and transferred to a 50 mL Teflon-lined stainless steel autoclave for solvothermal reaction at 240 °C for 24 h. The precursor solution is heated to the reaction temperature during the initial step of the solvothermal

https://doi.org/10.1021/acsaem.3c00887
ACS Appl. Energy Mater. 2023, 6, 6732−6741

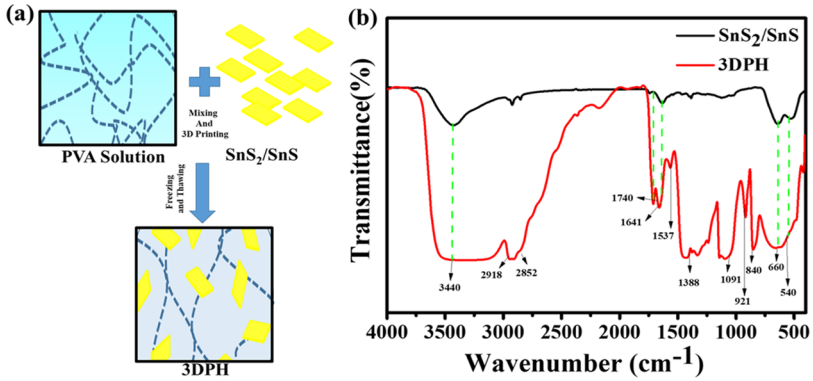

Figure 3. (a) Schematic of the PVA and SnS_2/SnS in 3DPH. (b) FTIR spectra of SnS_2/SnS and 3DPH.

process, which initiates the nucleation process. In that, the tin source (i.e., Sn^{4+} and Sn^{2+}) reacts with the sulfur source (i.e., S^{2-}) to generate nuclei, which are initially tiny and randomly distributed in the solution. The nuclei are produced as SnS_2/SnS due to the coexistence of Sn^{4+} and Sn^{2+}. The growth process, in which the nuclei expand into bigger crystals, occurs in the second stage. Under solvothermal synthesis conditions, the growth mechanism of SnS_2/SnS crystals may be characterized as a dissolution−precipitation process. The precursor solution provides a source of tin and sulfur ions, which dissolve the SnS_2/SnS crystals at the surface. Then, these ions diffuse through the solution and re-precipitate onto the crystal surface, resulting in crystal growth. After the reaction, the autoclave was cooled to ambient temperature (25 °C), and the as-obtained precipitate was centrifuged and washed repeatedly using DI water and ethanol till neutral pH. Then, it was dried under vacuum at 100 °C for 4 h to collect the SnS_2/SnS nanoflakes.

3.2. Preparation of the SnS_2/SnS/PVA Nanocomposite Solution. Two grams of PVA powder was homogeneously dissolved into 10 mL of DI water via continuous stirring at 85 °C. Later, the as-synthesized SnS_2/SnS powder was added to the PVA solution and stirred for 3 hrs, followed by 1 h of sonication to obtain a bubble-free homogeneous nanocomposite solution for 3D printing as shown in Figure 1b.

3.3. 3D Printing of the SnS_2/SnS/PVA Nanocomposite Hydrogel. A computer-aided design (CAD) model of the mesh-structured hydrogel was designed and sliced by Solidworks and Cura software, respectively. The as-prepared PVA nanocomposite solution was used to fabricate the PTNG device. In brief, the computer-programmed-controlled extrusion drive unit was attached to a solution container filled with the as-prepared nanocomposite solution, as shown in Supporting Information (SI) Figure S1. The force applied by the extrusion drive unit flows the nanocomposite solution toward the printer head over the conductive transparent ITO-coated PET sheet with a dimension of 2 cm × 2 cm. For example, 3D printing of the PVA solution is shown in SI Video V1. The nanocomposite solution was frozen inside the cooling chamber for 10 h at −23 °C, followed by thawing to room temperature. The cycle of the freezing and thawing process was performed five times to achieve PVA nanocomposite-based hydrogel (3DPH) for PTNG application, as shown in Figure 1c.

3.4. Customized Setup for the Measurement of PTNG. The real and schematic image of the customized setup for the measurement of the PTNG is shown in Supporting Information (SI) Figure S2. In brief, the 3D printed SnS_2/SnS-based hydrogel (3DPH) on the ITO/PET electrode was used as a tribo-positive material, while the copper foil was used as a tribo-negative material. Here, 3DPH on ITO/PET was attached to the glass slide, which was fixed to the sewing machine's movable upper clamp, and a copper foil was attached to the stator part, as shown in SI Figure S2a. The motion of the sewing machine causes uniform contact and separation between 3DPH and copper foil. Hence, a force of 3 ± 0.4 N was maintained throughout the experiment for a reliable reference in consistent force application. Further, a frequency of 120 cycles per minute, where the maximum separation distance was 30 mm in vertical contact separation mode, is maintained. The photoassisted measurements of the PTNG device were performed under light illumination, as shown in SI Figure S2b.

4. RESULTS AND DISCUSSION

4.1. Morphological and Structural Characterization of SnS_2/SnS. Figure 2a illustrates the SEM images of the solvothermal grown SnS_2/SnS. The SEM images demonstrate the irregular nanoflake-like structures of SnS_2/SnS with a minimum width of 20 ± 1 nm, which indicates the complete formation of differently sized SnS_2 and SnS from the amorphous tin and sulfur ions that were present in the precursors.[21] The SEM micrographs also depict the uniformly distributed SnS_2/SnS nanoflakes. The nanosize of SnS_2/SnS confirms the presence of more active sides, generating more electron−hole pairs during illumination in PTNG application. Figure 2b depicts the TEM micrographs of SnS_2/SnS, which validates the nanoflake-like morphology observed via SEM analysis. The TEM further confirms the existence of SnS_2 in nanoflakes via the (011) plane, as the interplanar distance for SnS_2 is observed to be ∼0.277. Figure 2c shows the selected area electron diffraction (SAED) pattern, which confirms the polycrystalline structure of SnS_2 and SnS. All these planes indicate the formation of the hexagonal and orthorhombic structures of SnS_2 and SnS in the SnS_2/SnS nanoflakes.

Figure 2d displays the X-ray diffraction (XRD) pattern of SnS_2/SnS. The diffraction peaks observed at 15.10, 28.20, 32.20, 42.00, and 50.11° correspond to the crystalline planes (001), (100), (011), (012), and (110), in good agreement with the JCPDS card No. 01-083-1705 for hexagonal SnS_2.[26] Additionally, the other diffraction peaks observed at 22.05, 26.03, 30.48, 31.90, 39.30, 44.85, 45.53, 48.70, 51.36, 52.60, 55.00, and 56.5° can be attributed to crystal planes of (101), (201), (011), (400), (410), (202), (020), (302), (511), (601), (610), and (420), respectively, which are also in agreement with the JCPDS card No. 01-73-1859 corresponding to orthorhombic SnS.[27]

For the optical properties of SnS_2/SnS, the sample was investigated by ultraviolet−visible (UV−vis) absorption spectroscopy, as shown in Figure 2f. At ∼640 nm wavelength, a high-intensity peak was observed, which explicated the maximum photoresponse of the SnS_2/SnS heterojunction in the visible spectra. Furthermore, the energy band gap (E_g) of SnS_2/SnS was examined using Tauc's equation (eq 1)[28]

$$(\alpha h\nu)^{1/2} = A(h\nu - E_g) \quad (1)$$

https://doi.org/10.1021/acsaem.3c00887
ACS Appl. Energy Mater. 2023, 6, 6732−6741

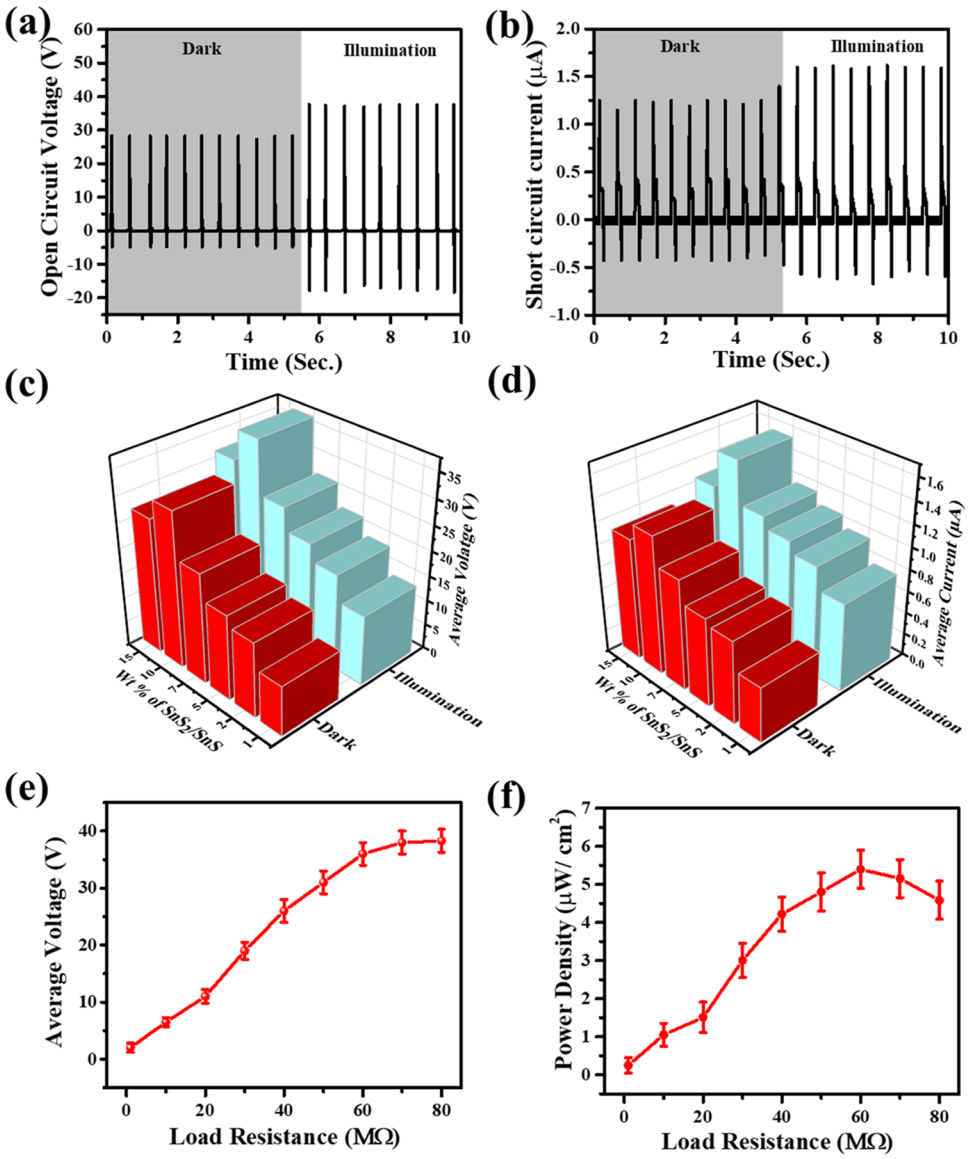

Figure 4. Output of PTNG in the dark and under illumination conditions: (a) open-circuit voltage (V_{oc}) and (b) short-circuit current (I_{sc}). The output of PTNG with different wt % of SnS_2/SnS in dark and illumination: (c) open-circuit voltage (V_{oc}) and (d) short-circuit current (I_{sc}). The output of PTNG with different load resistances under illumination: (e) voltage and (f) power density.

where $h\nu$ is the incident photon's energy and α is the absorption coefficient. As shown in Figure 2g, the band gap (E_g) of SnS_2/SnS was evaluated as 1.8 eV, which is lower than the previously reported SnS_2 and SnS/SnS_2 heterostructure.[21,29] This low-energy band gap will be more beneficial as the solar spectrum has low-energy light other than UV light, which is 5% of the total light.

Figure 3a shows the possible interaction of immobilization SnS_2/SnS nanoflakes in the PVA matrix and the formation of 3DPH in schematic representation. The freezing and thawing method results in cross-linking in the PVA matrix, thereby leading to the formation of 3DPH. The localization of the SnS_2/SnS nanoflakes within the gel network is visually identified by its uniform appearance. Figure 3b shows the Fourier transform infrared (FTIR) analysis, which was performed to understand the formation of 3DPH. The SnS_2/SnS nanoflakes and 3DPH were characterized by FTIR spectroscopy over the 400−4000 cm^{-1} range. The absorption peak at 3440 cm^{-1} in SnS_2/SnS nanoflakes represents O−H stretching. The broad absorption band at ∼3000−3600 cm^{-1} and a narrow peak at 921 cm^{-1} indicate O−H bonds in 3DPH. The absorption peaks at 2918 and 2852 cm^{-1} in 3DPH were assigned to CH and CH_2 asymmetric stretching vibration, respectively. The conjugate 1740 and 1641 cm^{-1} peaks represent the C═O and C═C stretching vibrations of 3DPH, respectively. The C═O vibrations show the presence of the vinyl acetate group of 3DPH. A small peak at 1537 cm^{-1} is attributed to the C═O stretching corresponding to the metal acetate functional group in 3DPH. Three strong peaks at 1388, 1091, and 840 cm^{-1} represent the C−OH, C−O, and C−C stretching vibrations in 3DPH, respectively. Further, the 660 cm^{-1} and 540 peaks were attributed to the Sn−S bond formation in SnS_2/SnS nanoflakes, which is also present in 3DPH. The peak broadening and overlapping peak in the FTIR for the 3DPH represents the cross-linking of the PVA hydrogel and SnS_2/SnS nanoflakes.[30]

4.2. Electrical Characterization of the Triboelectric Nanogenerator. The as-fabricated PTNG device was

https://doi.org/10.1021/acsaem.3c00887
ACS Appl. Energy Mater. 2023, 6, 6732−6741

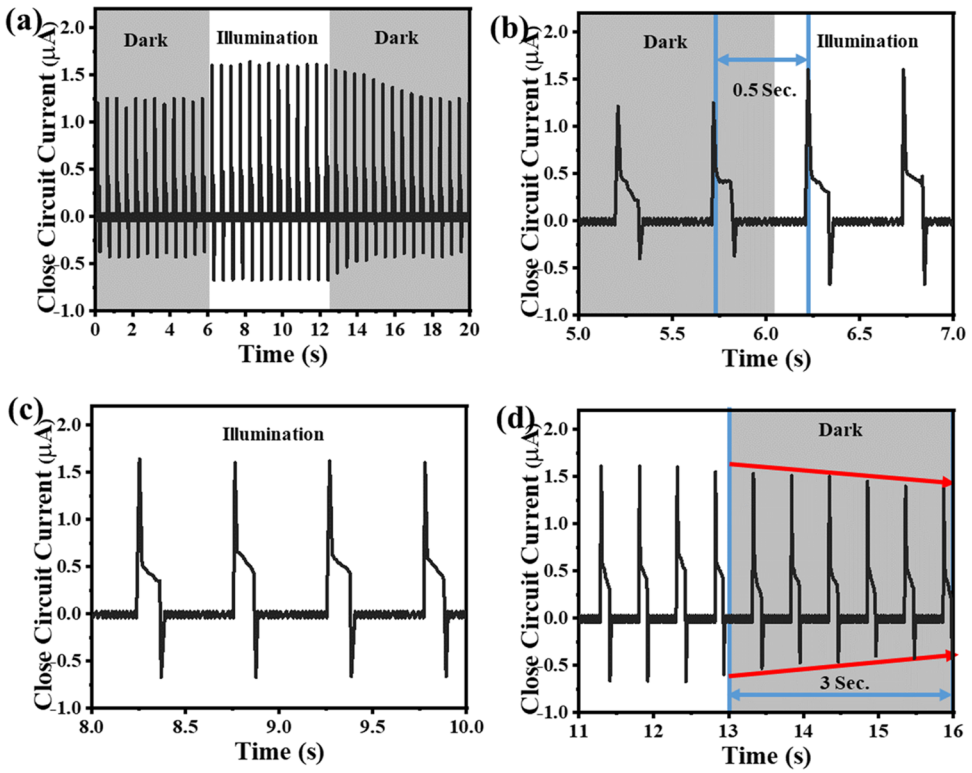

Figure 5. (a) I_{sc} of PTNG in the dark and under illumination. The enlarged plot of the PTNG corresponding to outputs at the moments of (b) light on, (c) continuous light illumination, and (d) light off.

examined under dark and illumination conditions to evaluate the hybridization effect, as shown in (Figure 4a,b). The device's response was initially observed in dark conditions for 5 s. Then, the light within the visible spectrum range was illuminated, and the corresponding response was measured. In the dark, the peak value of V_{oc} and I_{sc} of the PTNG was observed as 29 V and 1.23 μA, respectively. Under illumination, the V_{oc} and I_{sc} increased by 29 and 28% to 37.5 V and 1.58 μA, respectively, indicating the photomodulation of 3DPH. This increase in V_{oc} and I_{sc} can be attributed to photogenerated electron−hole pairs. The performance of the PTNG device at different wt % of SnS_2/SnS in 3DPH under the illumination of photons in terms of V_{oc} and I_{sc} was studied as depicted in Figure 4c,d, respectively. As the wt % of SnS_2/SnS (1−10 wt %) increased, the initial enhancement in output performance of the 3DPH-based PTNGs was observed till 10 wt %. Later, the fall in the output voltage trend observed at 15 wt % indicates that 10 wt % of the SnS_2/SnS-based PTNG device is an optimized high-performance device for energy harvesting applications. This rise and fall trend in the efficiency of PTNG with respect to wt % of SnS_2/SnS can be attributed to two vital factors as follows: (i) the change in dielectric constant and (ii) the piezoelectric property of SnS_2/SnS. The increase in the weight percentage of SnS_2/SnS up to 10% was observed to have an increasing trend in V_{oc} and I_{sc} output due to the formation of a microcapacitor interfacial network that led to an increase in the dielectric constant of 3DPH.[31] The decrease in the output of PTNG at 15 wt % of SnS_2/SnS can be attributed to the start of agglomeration, which caused the current leakage, leading to the deceased output of PTNG and the piezoelectric behavior of hydrogel caused by the inherent piezoelectric properties of SnS_2/SnS.[32]

Further, an experiment was performed to discuss the dependency of force on PTNG without light and by varying influencing factors like material thickness and active contact area under illumination as described in SI Section S1. Herein, the output of PTNG was measured by connecting various load resistors (R_{load}) with the external circuit. The average voltage output was measured by connecting the load resistor (1 to 80 MΩ) under illumination conditions, as shown in Figure 4e. From the figure, it can be easily observed that the voltage output increased with the increase in load resistance initially and saturated near 70 MΩ. The instantaneous power density was calculated by using

$$P = \frac{V^2}{R \times A} \tag{2}$$

where P is the power density, V is the average voltage output, R is the external load resistance, and A is the active area.

The output power of PTNG reached its highest when the load was near about 60 MΩ corresponding to 5.4 $\mu W \cdot cm^2$ (under illumination) as shown in Figure 4f. The long-term and cyclic stability test of PTNG has been explained in SI Section S2. To demonstrate the as-fabricated PTNG for practical applications, a 2.2 μF capacitor was connected to PTNG to be charged, which was further used to power light-emitting diodes (LEDs) and small electronic components like a calculator, as shown in SI Figure S6.

Figure 5a shows the photoresponse switching behavior while switching on and off the light. In the dark, the contact and separation of 3DPH and Cu generate I_{sc} of 1.25 μA by contact electrification and electrostatic induction. However, under illumination, the I_{sc} increased to 1.58 μA because of additional photoenergy, as shown in Figure 5b. The electron and holes generated by photoenergy increase the charge trapping by the

https://doi.org/10.1021/acsaem.3c00887
ACS Appl. Energy Mater. 2023, 6, 6732−6741

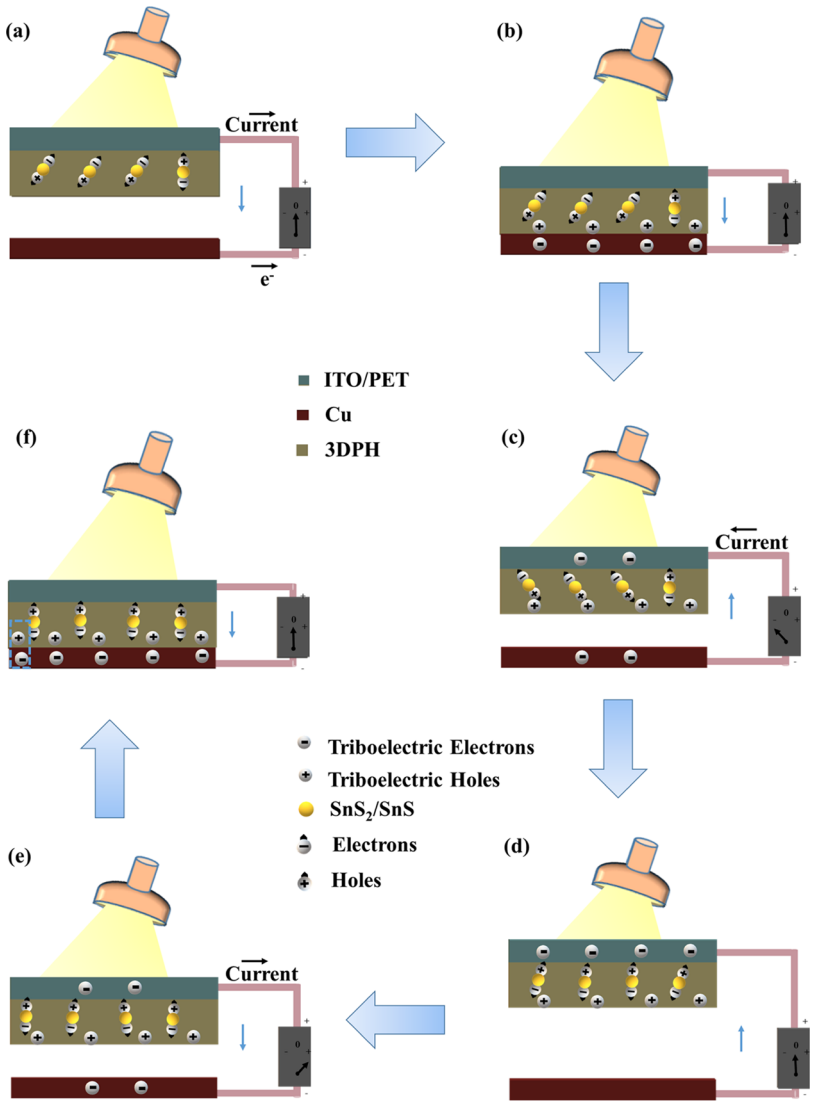

Figure 6. Working mechanism of PTNG under illumination for (a) no contact stage, (b) fully in contact stage, (c) initial stage of separation, (d) fully separation stage, (e) initial stage of the second cycle of contact, and (f) fully contact stage of the second cycle.

mutual coupling effect, which helps to accumulate more surface charges of 3DPH and Cu compared to dark mode. When the light source was switched on, the I_{sc} increased rapidly and stabilized at 1.58 μA, as depicted in Figure 5c. In the first response, it achieved a 28% increment and became saturated there. Therefore, the response time (time required to reach 90% of current deviation) can be calculated by the time difference between two peaks of I_{sc}, which is 0.5 s. Figure 5d illustrates the device's response after 6 s of illumination; when the light was turned off, the I_{sc} slowly reduced and recovered the previous dark as there was no more extra current generated under dark. The recovery time (the time difference to recover 90% of the current deviation or to recover up to 10% of the current increment) is calculated as 3 s, which is lesser than that of the previously reported triboelectric nanogenerator.[33]

4.3. Mechanism. The working mechanism of the as-fabricated PTNGs for the generation of V_{oc} and I_{sc} in the dark and under illumination conditions can be explained via the contact and separation processes, as shown in Figure 6. In the initial state, the PTNG does not create any electrical potential as there is no contact between two tribo-materials, i.e., 3DPH and Cu. When the external pushing force is applied, the transfer of positive and negative charges occurs in-between the surface of 3DPH and Cu because of the difference in surface charges, and both surfaces become charged identically.[13] In the separation process, the generated surface charges of 3DPH move toward the ITO electrode by two processes, i.e., (i) diffusion and (ii) electromigration, to balance the potential difference.[34] In the case of diffusion, the charge generated at the surface moves toward the inner space naturally because of the electrical charge concentration difference between the top surface and internal space of 3DPH. Along with diffusion, the charges move from the surface to the inner space of 3DPH due to the high difference in electric field strength between the surface of 3DPH and ITO. Due to this separation in 3DPH and Cu, the potential difference across the surfaces increased and drove the charges from the surface of Cu, which obtained a positive current in the external circuit. When the gap between 3DPH and Cu decreases, the potential difference between these two surfaces decreases; thus, the electrons from Cu flow back, resulting in a negative current.[19]

Photoactive semiconductor material with a low energy band gap generates the photocarriers under illumination. However, the recombination process of the electron−hole pairs from the

https://doi.org/10.1021/acsaem.3c00887
ACS Appl. Energy Mater. 2023, 6, 6732−6741

Table 1. Performance Comparison of the As-Fabricated PTNG with the Previously Reported Photoassisted Nanogenerators

tribo-material combination	band gap	output voltage (Illuminated)	output current (Illuminated)	device size	power density (Illuminated)	references
TiO_2 /FTO vs Au/glass	3.1 eV	0.45 V·cm^{-2} (V = 0.3 V)	35 nA·cm^{-2} (I = −28 nA)	1.4 cm × 0.8 cm	15.75 nW·cm^{-2}	19
$MAPbI_3/TiO_2$/FTO vs PTFE/FTO		4.25 V·cm^{-2} (V = 17 V)	0.09 μA· cm^{-2} (I = 0.38 μA)	2 cm × 2 cm	[a]0.38 μW·cm^{-2}	36
Al/polyimide/TiO_x/P3HT vs $PC_{61}BM$/PEDOT:PSS/ITO/glass		4 V·cm^{-2} (V = 4 V)	20 μA· cm^{-2} (I = 20 μA)	1 cm × 1 cm	[a]80 μW·cm^{-2}	37
Au/TiO_2/FTO vs TiO_2/FTO		0.7 V·cm (V ∼ 0.7 V)	11 μA· cm^{-2} (dark condition)	1 cm × 1 cm	not provided	38
$MA_{0.5}FA_{0.5}Pb_{0.5}Sn_{0.5}I_3$/FTO vs Al	1.24 eV	−58.33 V·cm^{-2} (V = −0.7 V)	100 μA· cm^{-2} (I = −1.2 μA)	0.012 cm^2	[a]5.8 mW·cm^{-2}	39
Si /Al vs FTO		0.35 V.cm^{-2} (V = 0.35 V)	0.25 μA· cm^{-2} (I = 0.25 μA)	1 cm × 1 cm	[a]0.08 μW·cm^{-2}	40
SnS_2/SnS and PVA 3D printed nanocomposite hydrogel vs Cu	2.1 eV for SnS_2/SnS	9.37 V·cm^{-2} (V = 37 V)	0.39 μA· cm^{-2} (I = 1.58 μA)	2 cm × 2 cm	5.4 μW·cm^{-2}	this work

[a]value calculated by using the formula, i.e., $P = V \cdot I$ (as resistance is constant).

carrier reduces the charge trap.[33] However, as per the quantum conversion efficiency theory, it has been concluded that the higher separation efficiency provides higher $I_{sc,}$ as the charge trap will be more.[35] In this work, the SnS_2/SnS acts as a photoactive material that boosts the efficiency of PTNG via a charge trap from the mutual coupling effect. In PTNG, the electron and holes, via the mutual coupling effect, can be excited from SnS_2/SnS within the triboelectric layer and distributed at the interface of 3DPH. When the charge accumulates on the surface of 3DPH and Cu due to mutual interaction, the electron−holes generated from mutual coupling effects are arranged vertically and trap the charge to enhance the efficiency of PTNG.[35] During the external force for the second time, the electric field will disappear, but the vertically arranged hole pairs will not entirely dissipate. In other words, under illumination, more charges will be accumulated on 3DPH and Cu, which results in a periodic higher current in the process of external periodical force.

Table 1 shows the performance comparison between the as-fabricated 3DPH-based PTNG and previously reported nanogenerators. Most reported PTNGs involved TiO_2 as a photoactive material combined with a variety of different materials and involved complex device architecture, which failed to achieve high efficiency due to the large energy band gap of TiO_2.[19,36−38] The high band gap value implies that TiO_2 can only respond to ultraviolet (UV) light, which accounts for less than 5% of the solar spectrum. In other reports for PTNGs, attempts were made to address the issue of large band gaps by using materials like perovskite, silicon, etc.[39,40] However, these exhibited either low stability and/or poor output performance. In sharp contrast, the as-fabricated SnS_2/SnS nanocomposite hydrogel PTNG demonstrated excellent stability and high performance than other reported PTNGs with its low energy band gap. This is the first report on 3DPH for PTNG application, exhibiting high V_{oc}, I_{sc}, and power density and excellent stability.

5. CONCLUSIONS

In summary, this work demonstrates a highly scalable approach of a 3D printed SnS_2/SnS-based nanocomposite hydrogel (3DPH) for photoinduced triboelectric nanogenerator (PTNG) application. Herein, the as-fabricated PTNG device exhibited high efficiency under illumination, which is ascribed to the narrow band gap of SnS_2/SnS in the matrix. The V_{oc} and I_{sc} of PTNG increased by about 29 and 28%, respectively, under light illumination, with 5.4 μW·cm^{-2} (under illumination) power density at 60 MΩ external resistance load. This enhancement is attributed to the migration of photogenerated charge carriers, which increases the charge-trapping capacity via the mutual coupling effect. This facile, low-cost technique of 3D printing nanocomposite hydrogel demonstrated here provides a new approach for the enhancement of mechanical-to-electrical conversion efficiency via photoinduced nanogenerator fabrication that finds wide applications in the development of next-generation self-powered systems.

■ ASSOCIATED CONTENT

Supporting Information

The Supporting Information is available free of charge at https://pubs.acs.org/doi/10.1021/acsaem.3c00887.

Digital photograph of a modified 3D printer (Figure S1); digital photograph and the corresponding schematic of the measurement setup for PTNG (Figure S2); the performance of PTNG by varying different influencing factors (Section S1); long-term and cyclic stability test of PTNG under illumination (Section S2); and digital photograph of the circuit connection to power LED and calculator (Figure S6) (PDF)

3D printing of the PVA solution (Video V1) (MP4)

■ AUTHOR INFORMATION

Corresponding Author

Sushmee Badhulika − *Department of Electrical Engineering, Indian Institute of Technology Hyderabad, Hyderabad 502285, India;* orcid.org/0000-0003-3237-3031; Phone: 040-23016467; Email: sbadh@iith.ac.in; Fax: 04023016032

Authors

Nishat Kumar Das − *Department of Electrical Engineering, Indian Institute of Technology Hyderabad, Hyderabad 502285, India;* orcid.org/0000-0002-5553-964X

Sushmitha Veeralingam − *Department of Electrical Engineering, Indian Institute of Technology Hyderabad, Hyderabad 502285, India*

Complete contact information is available at: https://pubs.acs.org/10.1021/acsaem.3c00887

Author Contributions

N.K.D. was responsible for conceptualization, methodology, data curation, writing the original draft, reviewing, and editing. S.V. performed the methodology and data curation and wrote, reviewed, and edited the manuscript. S.B. was responsible for conceptualization, funding acquisition, investigation, project administration, resources, supervision, and writing, reviewing, and editing the manuscript.

Notes

The authors declare no competing financial interest.

■ ACKNOWLEDGMENTS

S.B. acknowledges financial assistance from Defense Research Development Organization Young Scientist Laboratory-Asymmetric Technologies grant DYSL-AST/CARS/CONTRACT/20-21/02.

■ REFERENCES

(1) McManus, D.; Vranic, S.; Withers, F.; Romaguera, V. S.; Macucci, M.; Yang, H.; Sorrentino, R.; Parvez, K.; Son, S. K.; Iannaccone, G.; Kostarelos, K.; Fiori, G.; Casiraghi, C. Water-Based and Biocompatible 2D Crystal Inks for All-Inkjet-Printed Heterostructures. *Nat. Nanotechnol.* **2017**, *12*, 343−350.

(2) Gopalakrishnan, A.; Saha, R.; Vishnu, N.; Kumar, R.; Badhulika, S. Disposable, Efficient and Highly Selective Electrochemical Sensor based on Cadmium Oxide Nanoparticles Decorated Screen-Printed Carbon Electrode for Ascorbic Acid Determination in Fruit Juices. *Nano-Struct. Nano-Objects* **2018**, *16*, 96−103.

(3) Gross, B. C.; Erkal, J. L.; Lockwood, S. Y.; Chen, C.; Spence, D. M. Evaluation of 3D Printing and its Potential Impact on Biotechnology and the Chemical Sciences. *Anal. Chem.* **2014**, *86*, 3240−3253.

(4) Seol, M. L.; Han, J. W.; Moon, D., Il; Yoon, K. J.; Hwang, C. S.; Meyyappan, M. All-Printed Triboelectric Nanogenerator. *Nano Energy* **2018**, *44*, 82−88.

(5) Das, N. K.; Nanda, O. P.; Badhulika, S. Piezo/Triboelectric Nanogenerator from Lithium-Modified Zinc Titanium Oxide Nanofibers to Monitor Contact in Sports. *ACS Appl. Nano Mater.* **2023**, *6*, 1770−1782.

(6) Han, T.; Zhao, J.; Yuan, T.; Lei, D. Y.; Li, B.; Qiu, C. W. Theoretical Realization of an Ultra-Efficient Thermal-Energy Harvesting Cell Made of Natural Materials. *Energy Environ. Sci.* **2013**, *6*, 3537−3541.

(7) Zhang, C. L.; Yang, J. S.; Chen, W. Q. Low-Frequency Magnetic Energy Harvest using Multiferroic Composite Plates. *Phys. Lett. A* **2010**, *374*, 2406−2409.

(8) Shahi, P. K.; Singh, A. K.; Singh, S. K.; Rai, S. B.; Ullrich, B. Revelation of the Technological Versatility of the Eu(TTA)3Phen Complex by Demonstrating Energy Harvesting, Ultraviolet Light Detection, Temperature Sensing, and Laser Applications. *ACS Appl. Mater. Interfaces* **2015**, *7*, 18231−18239.

(9) Fan, F. R.; Tian, Z. Q.; Wang, Z. L. Flexible Triboelectric Generator. *Nano Energy* **2012**, *1*, 328−334.

(10) Shaw, P. E. Experiments on Tribo-Electricity. I.-the Tribo-Electric Series. *Proc. R. Soc. London, Ser. A* **1917**, *94*, 16−33.

(11) Khandelwal, G.; Minocha, T.; Yadav, S. K.; Chandrasekhar, A.; Raj, N. P. M. J.; Gupta, S. C.; Kim, S. J. All Edible Materials Derived Biocompatible and Biodegradable Triboelectric Nanogenerator. *Nano Energy* **2019**, *65*, No. 104016.

(12) Zhao, P.; Soin, N.; Prashanthi, K.; Chen, J.; Dong, S.; Zhou, E.; Zhu, Z.; Narasimulu, A. A.; Montemagno, C. D.; Yu, L.; Luo, J. Emulsion Electrospinning of Polytetrafluoroethylene (PTFE) Nanofibrous Membranes for High-Performance Triboelectric Nanogenerators. *ACS Appl. Mater. Interfaces* **2018**, *10*, 5880−5891.

(13) Das, N. K.; Ravipati, M.; Badhulika, S. Nickel Metal-Organic Framework/PVDF Composite Nanofibers based Self-Powered Wireless Sensor for Pulse Monitoring of Underwater Divers via Triboelectrically Generated Maxwell- Displacement Current. *Adv. Funct. Mater.* **2023**, 202303288.

(14) Sahatiya, P.; Kannan, S.; Badhulika, S. Few Layer MoS_2 and In-Situ Poled PVDF Nanofibers on Low Cost Paper Substrate as High Performance Piezo-Triboelectric Hybrid Nanogenerator: Energy Harvesting from Handwriting and Human Touch. *Appl. Mater. Today* **2018**, *13*, 91−99.

(15) Huang, S.; Shi, L.; Zou, T.; Kuang, H.; Rajagopalan, P.; Xu, H.; Zhan, S.; Chen, J.; Xuan, W.; Jin, H.; Dong, S.; Zhou, H.; Wang, X.; Yin, W.; Kim, J. M.; Luo, J. Controlling Performance of Organic−Inorganic Hybrid Perovskite Triboelectric Nanogenerators via Chemical Composition Modulation and Electric Field-Induced Ion Migration. *Adv. Energy Mater.* **2020**, *10*, No. 2002470.

(16) Kuang, H.; Li, Y.; Huang, S.; Shi, L.; Zhou, Z.; Gao, C.; Zeng, X.; Pandey, R.; Wang, X.; Dong, S.; Chen, X.; Yang, J.; Yang, H.; Luo, J. Piezoelectric Boron Nitride Nanosheets for High Performance Energy Harvesting Devices. *Nano Energy* **2021**, *80*, No. 105561.

(17) Pradel, K. C.; Fukata, N. Systematic Optimization of Triboelectric Nanogenerator Performance through Surface Micropatterning. *Nano Energy* **2021**, *83*, No. 105856.

(18) Su, L.; Zhao, Z.; Li, H. Y.; Yuan, J.; Wang, Z. L.; Cao, G. Z.; Zhu, G. High-Performance Organolead Halide Perovskite-Based Self-Powered Triboelectric Photodetector. *ACS Nano* **2015**, *9*, 11310−11316.

(19) Han, J.; Yang, X.; Liao, L.; Zhou, G.; Wang, G.; Xu, C.; Hu, W.; Debora, M. E. R.; Song, Q. Photo-induced Triboelectric Polarity Reversal and Enhancement of a New Metal/Semiconductor Triboelectric Nanogenerator. *Nano Energy* **2019**, *58*, 331−337.

(20) Yu, Z.; Yang, H.; Soin, N.; Chen, L.; Black, N.; Xu, K.; Sharma, P. K.; Tsonos, C.; Kumar, A.; Luo, J. Bismuth Oxyhalide based Photo-Enhanced Triboelectric Nanogenerators. *Nano Energy* **2021**, *89*, No. 106419.

(21) Yao, K.; Li, J.; Shan, S.; Jia, Q. One-Step Synthesis of Urchinlike SnS/SnS_2 Heterostructures with Superior Visible-Light Photocatalytic Performance. *Catal. Commun.* **2017**, *101*, 51−56.

(22) Gao, L.; Liu, C.; Meng, F.; Liu, A.; Li, Y.; Li, Y.; Zhang, C.; Fan, M.; Wei, G.; Ma, T. Significantly Enhanced V-oc and Efficiency in Perovskite Solar Cells through Composition Adjustment of SnS_2 Electron Transport Layers. *ACS Sustainable Chem. Eng.* **2020**, *8*, 9250−9256.

(23) Shinde, P.; Rout, C. S. Advances in Synthesis, Properties and Emerging Applications of Tin Sulfides and its Heterostructures. *Mater. Chem. Front.* **2021**, *5*, 516−556.

(24) Zhang, J.; Jiao, B.; Dai, J.; Wu, D.; Wu, Z.; Bian, L.; Zhao, Y.; Yang, W.; Jiang, M.; Lu, S. Enhance the Responsivity and Response Speed of Self-Powered Ultraviolet Photodetector by GaN/$CsPbBr_3$ Core-Shell Nanowire Heterojunction and Hydrogel. *Nano Energy* **2022**, *100*, No. 107437.

(25) Mousavi, S. S.; Sajad, B.; Majlesara, M. H. Fast Response Zno/Pva Nanocomposite-based Photodiodes Modified by Graphene Quantum Dots. *Mater. Des.* **2019**, *162*, 249−255.

(26) Lakshmi, V.; Chen, Y.; Mikhaylov, A. A.; Medvedev, A. G.; Sultana, I.; Rahman, M. M.; Lev, O.; Prikhodchenko, P. V.; Glushenkov, A. M. Nanocrystalline SnS2 Coated onto Reduced Graphene Oxide: Demonstrating the Feasibility of a Non-Graphitic Anode with Sulfide Chemistry for Potassium-Ion Batteries. *Chem. Commun.* **2017**, *53*, 8272−8275.

(27) Biacchi, A. J.; Vaughn, D. D.; Schaak, R. E. Synthesis and Crystallographic Analysis of Shape-Controlled SnS Nanocrystal Photocatalysts: Evidence for a Pseudotetragonal Structural Modification. *J. Am. Chem. Soc.* **2013**, *135*, 11634−11644.

(28) Veeralingam, S.; Durai, L.; Badhulika, S. Facile Fabrication of P(Electrodeposition)/N(Solvothermal) 2D-WS_2-Homojunction Based High Performance Photo Responsive, Strain Modulated Piezo-Phototronic Diode. *ChemNanoMat* **2019**, *5*, 1521−1530.

(29) Veeralingam, S.; Badhulika, S. Coaxial SnS_2/SnS Nanostructures on the Ag Fiber Substrate for Flexible Self-Powered Photodetectors. *ACS Appl. Nano Mater.* **2023**, *6*, 3863−3872.

https://doi.org/10.1021/acsaem.3c00887
ACS Appl. Energy Mater. 2023, 6, 6732−6741

(30) Mansur, H. S.; Sadahira, C. M.; Souza, A. N.; Mansur, A. A. P. FTIR Spectroscopy Characterization of Poly (Vinyl Alcohol) Hydrogel With Different Hydrolysis Degree and Chemically Crosslinked with Glutaraldehyde. *Mater. Sci. Eng.: C* **2008**, *28*, 539−548.
(31) Luo, X.; Zhu, L.; Wang, Y. C.; Li, J.; Nie, J.; Wang, Z. L. A Flexible Multifunctional Triboelectric Nanogenerator Based on MXene/PVA Hydrogel. *Adv. Funct. Mater.* **2021**, *31*, No. 2104928.
(32) Cao, V. A.; Kim, M.; Hu, W.; Lee, S.; Youn, S.; Chang, J.; Chang, H. S.; Nah, J. Enhanced Piezoelectric Output Performance of the SnS_2/SnS Heterostructure Thin-Film Piezoelectric Nanogenerator Realized by Atomic Layer Deposition. *ACS Nano* **2021**, *15*, 10428−10436.
(33) Chakraborty, I.; Wu, M. C.; Lai, S. N.; Lai, C. S. Self-Powered Broadband Photodetection with Mixed-Phase Black TiO_2-Assisted Output Boosting of a Biobased Triboelectric Nanogenerator. *Chem. Eng. J.* **2023**, *452*, No. 139138.
(34) Choi, J. H.; Ra, Y.; Cho, S.; La, M.; Park, S. J.; Choi, D. Electrical Charge Storage Effect in Carbon Based Polymer Composite for Long-Term Performance Enhancement of the Triboelectric Nanogenerator. *Compos. Sci. Technol.* **2021**, *207*, No. 108680.
(35) Chen, X.; Zhao, Y.; Wang, F.; Tong, D.; Gao, L.; Li, D.; Wu, L.; Mu, X.; Yang, Y. Boosting Output Performance of Triboelectric Nanogenerator via Mutual Coupling Effects Enabled Photon-Carriers and Plasmon. *Adv. Sci.* **2022**, *9*, No. 2103957.
(36) Su, L.; Zhao, Z.; Li, H.; Wang, Y.; Kuang, S.; Cao, G.; Wang, Z.; Zhu, G. Photo-induced Enhancement of a Triboelectric Nanogenerator Based on an Organolead Halide Perovskite. *J. Mater. Chem. C* **2016**, *4*, 10395−10399.
(37) Ye, B. U.; Lee, S. Y.; Jung, M.; Sohn, S. D.; Shin, H. J.; Song, M. H.; Choi, K. J.; Baik, J. M. Photo-Stimulated Triboelectric Generation. *Nanoscale* **2017**, *9*, 18597−18603.
(38) Han, G. H.; Lee, J. P.; Kim, H. J.; Shin, J.; Baik, J. M. Photostimulated charge transfer in contact electrification coupled with plasmonic excitations. *Nano Energy* **2019**, *65*, No. 104031.
(39) Hao, Z.; Jiang, T.; Lu, Y.; Feng, S.; Shen, R.; Yao, T.; Yan, Y.; Yang, Y.; Lu, Y.; Lin, S. Co-harvesting Light and Mechanical Energy Based on Dynamic Metal/Perovskite Schottky Junction. *Matter* **2019**, *1*, 639−649.
(40) Liu, J.; Zhang, Y.; Chen, J.; Bao, R.; Jiang, K.; Khan, F.; Goswami, A.; Li, Z.; Liu, F.; Feng, K.; Luo, J.; Thundat, T. Separation and Quantum Tunneling of Photogenerated Carriers Using a Tribo-Induced Field. *Matter* **2019**, *1*, 650−660.

https://doi.org/10.1021/acsaem.3c00887
ACS Appl. Energy Mater. 2023, 6, 6732−6741